Original Paper

Nucleation and crystallization kinetics on float glass surfaces

Joachim Deubener, Rolf Brückner and Heiko Hessenkemper[1])
Institut für Nichtmetallische Werkstoffe – Anorganische Werkstoffe –, Technische Universität Berlin (FRG)

The superficial crystallization kinetics of a commercial float glass is investigated in the temperature range from 665 to 925 °C. The following phases were observed: cristobalite, devitrite, sporadically sodium metasilicate and additionally β-wollastonite if a reducing atmosphere is applied.

The devitrification process is divided into a primary crystallization of cristobalite and a secondary appearance of devitrite after an induction time ($t > 7$ min). The growth rates of devitrite are up to 4 times larger than those of cristobalite, thus, a fractured surface perpendicular to the float glass plate shows a two-stage devitrification image after longer times of heat treatment. The growth rates depend on the furnace atmosphere as well as on the compositional variations of the two float glass surfaces.

The activation enthalpies of crystal growth rates are (in kJ/mol): $\approx$ 110 for cristobalite, $\approx$ 150 for β-wollastonite and $\approx$ 220 for devitrite. A superficial phase separation occurs at the tin bath side if oxidizing furnace atmosphere is applied. This can be related to a redox interaction of the tin ions and has consequences on nucleation, induction period, crystal growth mechanism and "bloom" effect.

Heterogeneous surface nucleation arises from a certain number of sites which are specific for the various crystal phases. In the case of cristobalite the time and temperature dependence of the number of crystals are measured and nucleation rates were determined on the atmosphere side under oxidizing conditions.

Keimbildungs- und Kristallisationskinetik auf Floatglasoberflächen

Die Oberflächenkristallisationskinetik eines handelsüblichen Floatglases wird im Temperaturbereich von 665 bis 925 °C untersucht. Folgende Phasen wurden erhalten: Cristobalit, Devitrit, sporadisch Natriummetasilicat und zusätzlich β-Wollastonit, wenn die Wärmebehandlung in reduzierender Atmosphäre vorgenommen wird.

Der Entglasungsprozeß beginnt mit einer primären Kristallisation von Cristobalit, dem nach der Induktionsperiode von $t > 7$ min eine Sekundärkristallisation von Devitrit folgt. Die Wachstumsgeschwindigkeit des Devitrits ist bis zu viermal größer als die des Cristobalits, so daß die Bruchflächen senkrecht zur Floatglasoberfläche den Eindruck einer Zweistufenkristallisation nach längerer Wärmebehandlungszeit vermitteln. Die Wachstumsraten hängen sowohl von der Ofenatmosphäre als auch von der unterschiedlichen chemischen Zusammensetzung der beiden Floatglasoberflächen ab.

Die Aktivierungsenthalpien der Kristallwachstumsraten betragen (in kJ/mol) für Cristobalit $\approx$ 110, für β-Wollastonit $\approx$ 150 und für Devitrit $\approx$ 220. Auf der Zinnbadseite wird in oxidierender Ofenatmosphäre eine Oberflächenentmischung beobachtet, die auf eine Redoxwechselwirkung der Zinnionen zurückgeführt wird und die Keimbildung, Induktionsperiode, den Kristallwachstumsmechanismus und den „bloom"-Effekt beeinflußt.

Die Keimbildung an der Oberfläche ist heterogen und rührt von einer bestimmten Anzahl von Stellen her, die für die verschiedenen Kristallphasen spezifisch sind. Im Fall des Cristobalits wurden Zeit- und Temperaturabhängigkeit der Kristallitanzahl gemessen und die Keimbildungsgeschwindigkeit auf der Atmosphärenseite unter oxidierenden Bedingungen bestimmt.

1. Introduction

Two surface layers with different chemical compositions and physical properties are produced during the float glass process, they show an impoverishment of the surface layers in alkali, alkaline earth and hydroxyl ions which is partly compensated by tin ions on the tin bath side [1]. A review of previous research demonstrates that the thickness of the reaction layers is in the order of 8 to 40 µm [1 to 5]. This causes compressive surface stresses which are larger on the atmosphere than on the tin bath side. This again leads to 20 % larger flexural strength values if the atmosphere side is under tensile stress [6]. Merker [7] observed that float glass surface layers have also different Fe^{2+}/Fe^{total} ratios as compared to the bulk glass due to variations of the redox conditions. Recently Matoušek and Maryška [8] detected a different surface interaction of the float glass layers with potassium, silver and copper salt melts. Finally, the two float glass surfaces show a different chemical resistance against water [9 and 10].

First experiments on surface crystallization pointed out that the thickness of crystallization layers of the atmosphere side is also different from that of the tin bath side (figures 1a and b). The goal of the present work is therefore to investigate the crystallization behaviour on the two float glass surfaces in more detail.

Received November 21, 1991.
[1]) Now with: Gerresheimer Glas AG, Achern (FRG).

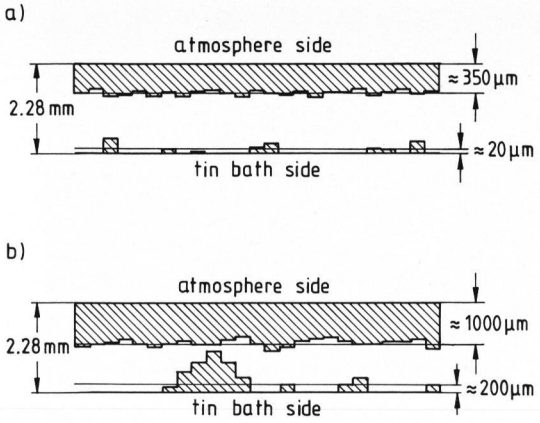

Figures 1a and b. Continuous crystalline layer at the atmosphere side of float glass and some crystalline spots at the tin bath side (schematically); a) $\vartheta = 770\,°C$, $t = 50$ h; b) $\vartheta = 830\,°C$, $t = 24$ h.

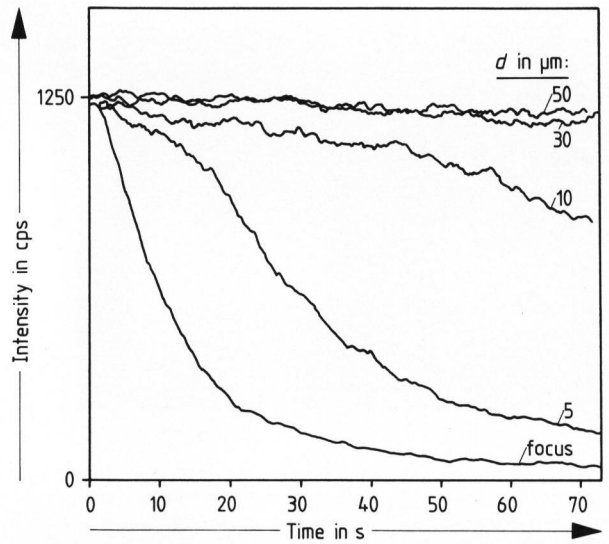

Figure 2. Intensity of X-ray Na-K_α (15 kV, 20 mA) from float glass surface versus time at various focus diameters, d, of the electron beam in the Cameca microprobe.

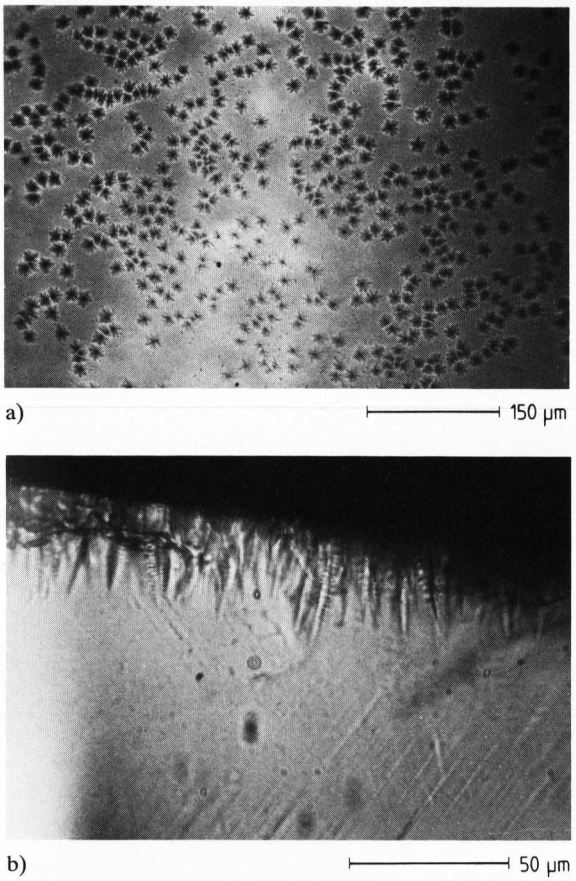

Figures 3a and b. Optical micrographs of heat-treated float glass samples with cristobalite crystals; a) spherical symmetry, bulk glass surface, $\vartheta = 905\,°C$, $t = 30$ min; b) fir-tree shape, atmosphere side of float glass, fracture perpendicular to the float glass surface, $\vartheta = 775\,°C$, $t = 15$ h.

2. Experimental

A plate of commercial float glass ($d = 2.28$ mm) was cut into samples of (7×50) mm^2 and cleaned in an alcohol/acetone ultrasonic bath. The difference between the tin bath and the atmosphere side was determined by a tin fluorescence test. Other samples were ground (about 0.3 mm) and polished in order to get the bulk glass composition at the surface.

In this way three parts of the float glass could be investigated: the atmosphere side, the tin bath side and the bulk glass surface. The chemical compositions were determined by electron microprobe technique (Camebax-microbeam, Cameca, Paris (France)) with a defocused electron beam in such a way that no change of the sodium concentration could be observed. Figure 2 demonstrates that this is the case, if the focus is not smaller than 30 µm in diameter. The information depth of the analytical results is about 1 to 2 µm, 90 % from 2 µm and 60 % from 1 µm depth.

The crystallization experiments were carried out in a gradient tube furnace controlled accurately to within 1 K of the heat treatment temperature in air or in a strong reducing atmosphere (H_2/N_2 flow). After heat treatment the glasses were examined with the help of an optical microscope in connection with an image-analyzing computer at magnifications of up to 1250fold. The crystallizing phases were identified by optical methods and X-ray diffraction (XRD). The following parameters were determined: v, the crystal growth rate; t, the induction time for surface crystallization and N_s, the average number of crystals per unit area from surface nucleation.

3. Results

Within the temperature range from 665 to 925 °C only surface crystallization was observed. The following crystallizing phases at the atmosphere side, tin bath side and at the bulk glass surface were observed: cristobalite, devitrite, sporadically sodium metasil-

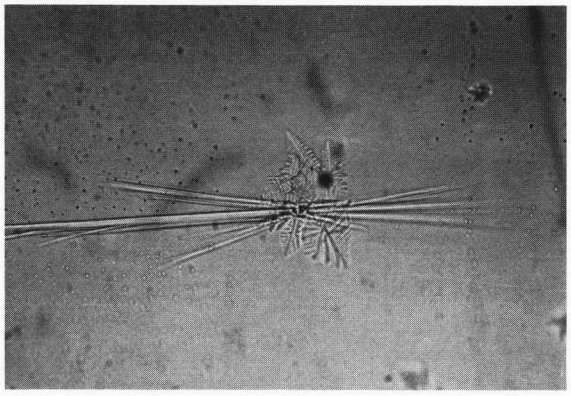

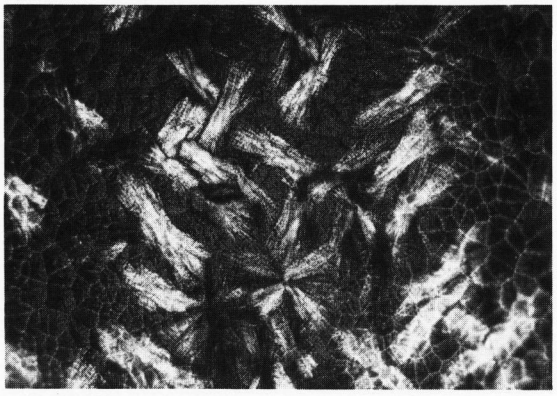

Figures 4a and b. Optical micrographs of heat-treated float glass samples with devitrite crystals; a) needle-like appearance and cristobalite, dendritic appearance, tin bath side, grown in N_2/H_2 atmosphere, $\vartheta = 857\,°C$, $t = 45$ min; b) spherulites of devitrite below a layer of cristobalite (under crossed Nicols) on the bulk glass surface, $\vartheta = 855\,°C$, $t = 75$ min.

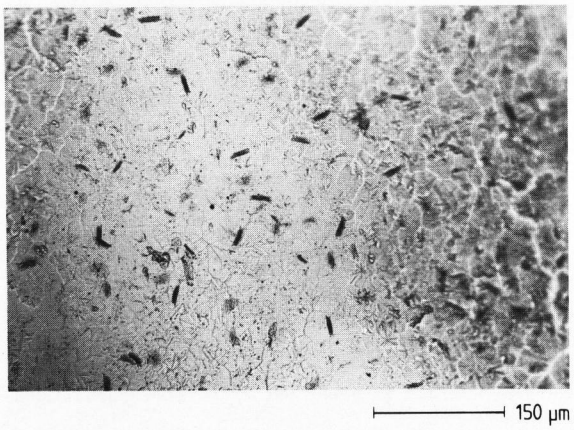

Figure 5. Optical micrograph of a heat-treated float glass sample with β-wollastonite (beam-like crystals) and cristobalite on bulk glass surface grown in N_2/H_2 atmosphere, $\vartheta = 893\,°C$, $t = 75$ min.

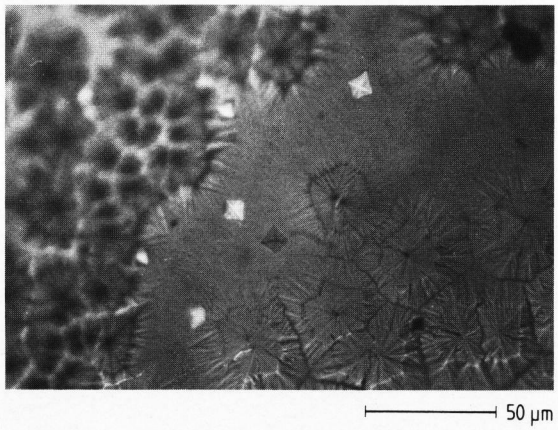

Figure 6. Optical micrograph of a heat-treated float glass sample (under crossed Nicols) with sodium metasilicate (bipyramidal crystals) and cristobalite on atmosphere side surface, $\vartheta = 917\,°C$, $t = 75$ min.

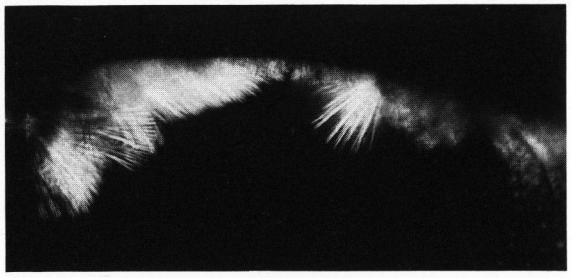

◀ Figures 7a and b. Optical micrographs of heat-treated float glass samples with dominating devitrite crystallization; a) needle-like crystals with cristobalite, dendritic appearance (small crystals), cross-sectional surface, $\vartheta = 896\,°C$, $t = 90$ min; b) two-stage devitrification image of a cross-sectional surface: spherulites of devitrite and fir-tree shaped cristobalite (under crossed Nicols), $\vartheta = 898\,°C$, $t = 240$ min.

icate (XRD: $Na_2O \cdot SiO_2 \cdot nH_2O$, $n = 0.5$) and additionally β-wollastonite if reducing atmosphere was applied.

3.1. Crystal growth morphology

Cristobalite:

Cristobalite represents a high-temperature modification of pure silica which transforms to tridymite with a certain content of impurity ions [11]. The optical properties and the growth morphology are altered by the degree of transformation. In the early stage of crystallization three-fold and six-fold star-like crystals

were observed at the surface. With longer heat treatment the initial crystals show spherical symmetry, although only X-ray peaks belonging to cristobalite were detected (figure 3a). Perpendicular to the float glass surface the growth morphology especially changed to a dendritic appearance with a characteristic fir-tree shape (figure 3b).

Devitrite:

Small elongated needle-like crystals were observed, growing to spherulites after longer periods of heat treatment (figures 4a and b).

β-Wollastonite:

Flat beam-like crystals were formed if reducing atmosphere was applied (figure 5).

Sodium metasilicate:

Sodium metasilicate respectively sodium–metasilicate hydrate was observed sporadically in form of the bipyramidal crystals (figure 6). The influence of sodium metasilicate on the devitrification process was negligibly small and no further investigations were carried out.

3.2. Devitrification processes

3.2.1. Devitrification at the atmosphere side

The devitrification process may be divided into two steps: The first step is represented by primary crystallization of cristobalite. The second step starts after an induction time (at least 7 min) by crystallization of devitrite. The measured growth rates of devitrite are up to 4 times larger as compared with that of cristobalite. According to this effect devitrite quickly controls the devitrification development (figures 7a and b).

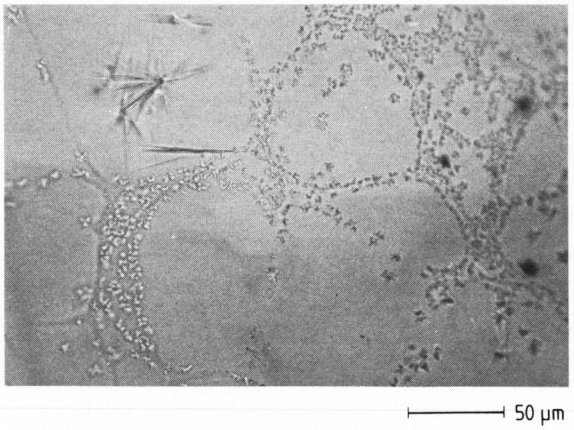

Figure 8. Optical micrograph of a heat-treated float glass sample with superficial phase separation on the tin bath side: devitrite (needle-like crystals) and cristobalite (preferential on the boundaries between the circular sections), $\vartheta = 910\,°C$, $t = 45$ min.

The additional presence of β-wollastonite in reducing atmosphere after an induction time similar to devitrite has only little influence on the devitrification process, because the measured growth rates are smaller as compared with those of cristobalite.

3.2.2. Devitrification at the tin bath side

After a few minutes of heat treatment in air within the investigated temperature range the surface of the tin

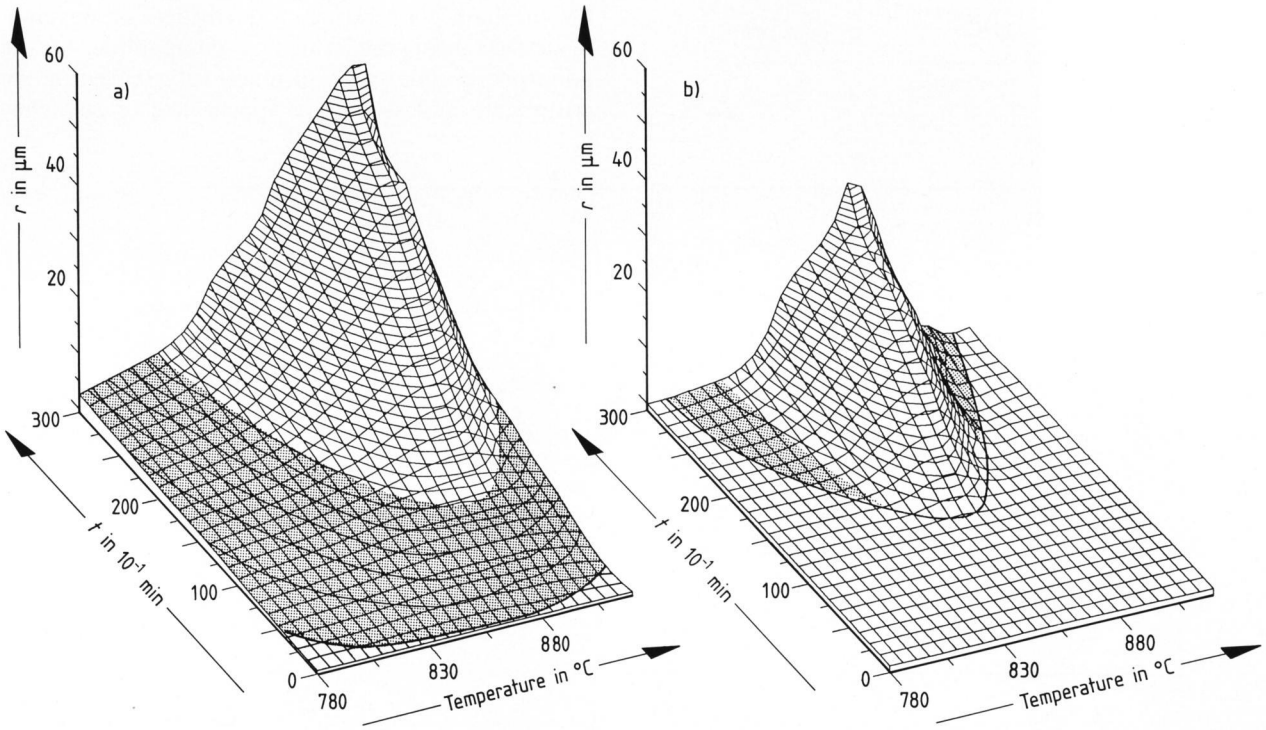

Figures 9a and b. Three-dimensional plot of the radius of the largest crystal dimension at a) atmosphere side, b) tin bath side (in air). Shadowed area: cristobalite, unshadowed area: devitrite.

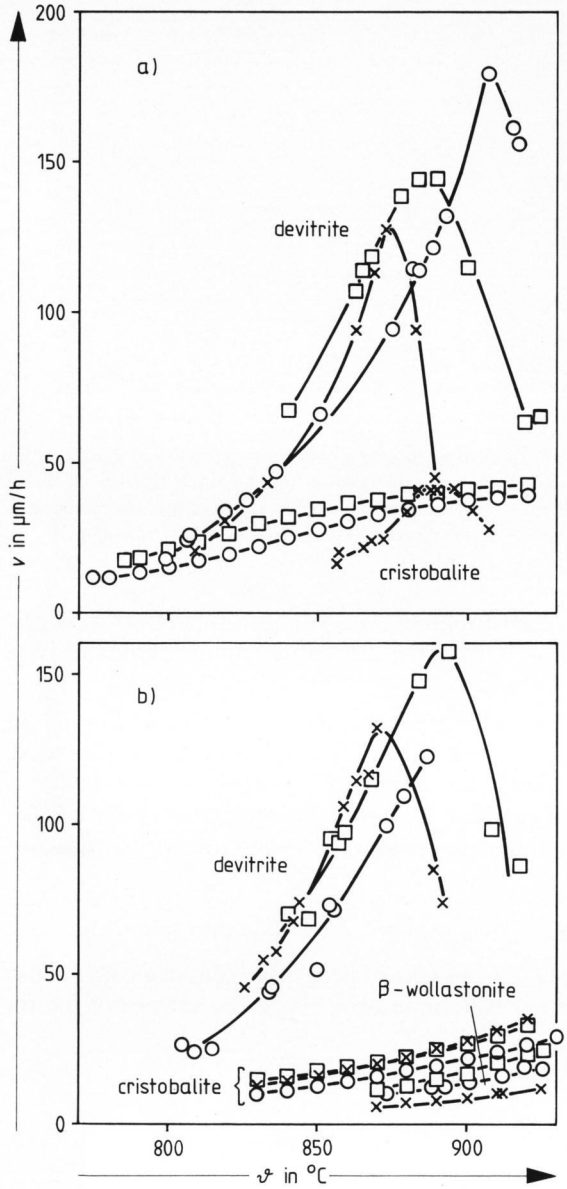

◀ Figures 10a and b. Crystal growth rates versus temperature of a) devitrite and cristobalite in air; b) devitrite, cristobalite and β-wollastonite in reducing atmosphere (N_2/H_2 flow). ×: tin bath side, ○: atmosphere side, □: bulk glass surface.

bath side exhibits a phase separation structure. In this early stage no crystallization was observed. The appearance of this liquid-phase separation on the surface of the tin bath side for samples which had been heat-treated in air changed the order of devitrification. Primary crystallization of devitrite ($\vartheta \approx 850$ °C) particularly occurred in the separated circular sections after an induction time of at least 10 min followed by cristobalite preferentially at the boundaries between the circular sections with reduced nucleation and growth rates (figure 8). The consequence for this devitrification process is a decreased fractional crystallized volume as shown in figures 1a and b.

If reducing furnace atmosphere was applied no superficial immiscibility was observed and the crystallization process obeys the sequence discussed in section 3.2.1.

To explain the differences between the devitrification development at the tin bath and the atmosphere side of the float glass (furnace atmosphere: air) three-dimensional plots are shown in figures 9a and b based on 244 measured values of r (the radius of the largest crystal dimension) for each plot.

3.2.3. Devitrification at the bulk glass surface

On the bulk glass surface a devitrification development was observed which is comparable to the atmosphere side with primary crystallization of cristobalite and secondary appearance of devitrite.

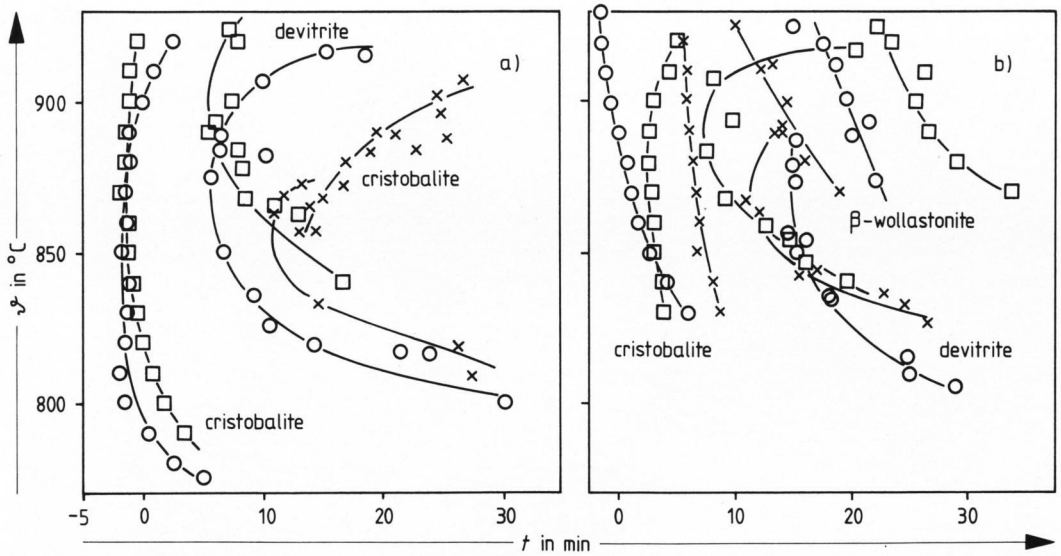

Figures 11a and b. Induction time versus temperature of a) devitrite and cristobalite in air; b) devitrite, cristobalite and β-wollastonite in reducing atmosphere (N_2/H_2 flow). ×: tin bath side, ○: atmosphere side, □: bulk glass surface.

3.3. Growth rates and induction times

The measured growth rates are shown in figures 10a and b. They were determined by measuring the length of the largest crystal dimension and the time intervals between successive heat treatments. The growth rates were time-independent and closely correlated with interface morphologies. A least-squares linear regression analysis was applied to fit the best straight line for the growth data. The growth rates of devitrite show a variation of the maxima in the order: tin bath, bulk glass and atmosphere side towards increasing temperature and maximum growth rates. In contrast to devitrite, cristobalite exhibits considerably lower growth rates if reducing atmosphere is used (figures 10a and b).

In an oxidizing furnace atmosphere the growth behaviour of cristobalite on the tin bath side differs significantly from the expected trend as a consequence of the observed phase separation.

The induction times, t, were determined from the intercepts on the time axis of the crystal length versus time of heat treatment plots. They are presented in figures 11a and b. Negative values of t are due to a post-growing effect because the samples had been quenched only in air. This quenching time was not short enough to avoid crystal growth totally after heat treatment.

3.4. Nucleation

A representative selection of the nucleation results for cristobalite is shown in figure 12 from which can be seen that the average number of crystals per unit area, N_s, due to surface nucleation on the atmosphere side of the float glass exhibits a non-linear behaviour. At elevated temperatures (for example 900 °C) the diagram shows a saturation effect, whereas at lower temperatures (678 °C) a transient behaviour is observed which will be discussed in section 4.3.

In a similar way the nucleation was studied for devitrite and β-wollastonite. The following series of maximum values of N_s on the atmosphere side were measured in air: cristobalite up to 2400, devitrite up to 15 and β-wollastonite up to 40 mm^{-2}.

3.5. A non-crystalline alteration at the surface

A wavy structure of the glass surface at the tin bath side was observed after a prolonged annealing time in air. Figure 13 shows this phenomenon after a period of 20 h at 730 °C. These wavy shrinking structures are totally glassy and have been described by Pilkington [12] who called this phenomenon "bloom".

4. Discussion

4.1. Enthalpies, crystal growth rates and influence of compositional changes

At large undercooling temperatures, below the maxima of growth rates, v, a plot of ln v versus $1/T$ should yield a straight line with a slope proportional to ΔH_D, where ΔH_D is the activation enthalpy of crystal growth (figures 14a and b). A summary of the results is given in table 1. The activation enthalpy of cristobalite at the atmosphere side (about 110 kJ/mol) is in good agreement with data of Dietzel and Wickert [13] and Schönborn [14]. These authors studied surface crystallization in several alkali silicate and borosilicate glasses. From their data the activation enthalpy of cristobalite had been calculated to be 110 kJ/mol in alkali silicate glasses and 100 to 135 kJ/mol in borosilicate glasses, respectively.

On the tin bath side in the case of crystallization of cristobalite in air ΔH_D (285 kJ/mol) is 2 to 3 times larger than the values at the atmosphere side reflecting a drastic change in growth mechanism.

The activation enthalpies of devitrite in several soda–lime–silica glasses had been calculated from the data of Dietzel and Flörke [15] and Swift [16] to be 210 to 275 kJ/mol. These values fit well with the measured activation enthalpies of devitrite at the surfaces of float glass.

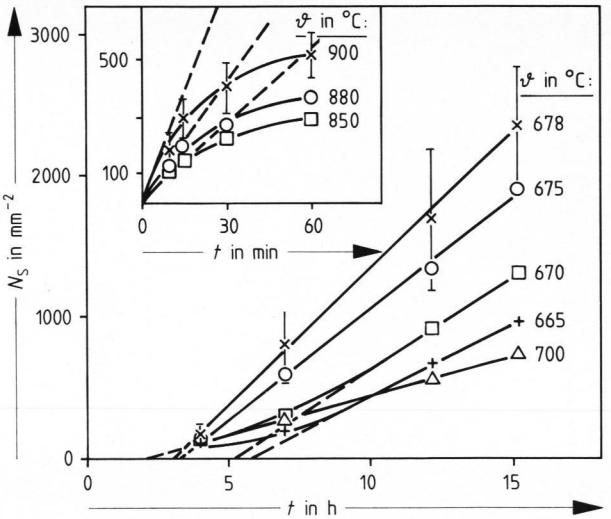

Figure 12. Average number of cristobalite crystals per unit area in air from surface nucleation (atmosphere side) versus time at various temperatures.

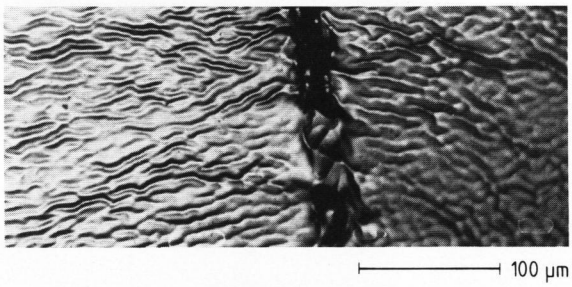

Figure 13. Optical micrograph of a heat-treated float glass sample with wavy shrinking structures at the tin bath side after $t = 20$ h at $\vartheta = 730$ °C.

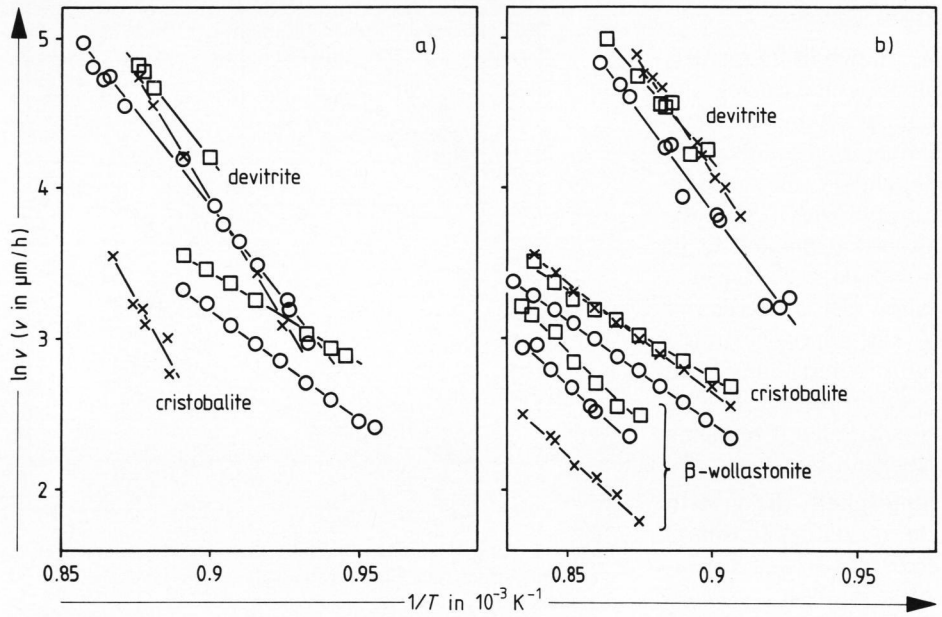

Figures 14a and b. Arrhenius plots of crystal growth rates versus $10^3/T$ of a) devitrite and cristobalite in air; b) devitrite, cristobalite and β-wollastonite in reducing atmosphere (N_2/H_2 flow). ×: tin bath side, ○: atmosphere side, □: bulk glass surface.

Table 1. Enthalpies of crystal growth, ΔH_D, (in kJ/mol) of cristobalite, devitrite, and β-wollastonite in oxidizing (air) and reducing atmosphere (N_2/H_2) on the surfaces of float glass

	furnace atmosphere	tin bath side	atmosphere side	bulk glas surface
cristobalite	air	285	121	102
	N_2/H_2	119	113	97
devitrite	air	280	209	216
	N_2/H_2	247	217	197
β-wollastonite	air	–	–	–
	N_2/H_2	143	142	161

A comparison of the activation enthalpies in table 1 shows with the exception of the value for cristobalite at the tin bath side that the values increase with increasing number of components: $SiO_2 \rightarrow CaO \cdot SiO_2 \rightarrow Na_2O \cdot CaO \cdot SiO_2$. These data are significantly lower than the Si–O bonding energy which was determined by Kuan Han-Sun [17] to be 444 kJ/mol but they are in the order of magnitude for the Ca–O (134 kJ/mol) and Na–O bonding energy (83 kJ/mol). As a conclusion the activation enthalpies of crystal growth of float glass excludes a fracture of Si–O bonds during crystallization of the three phases but allows the fracture of Ca–O and Na–O bonds. This is valid for all sides of the float glass (table 1).

Another comparison is given in table 1. Starting from the enthalpy values of the bulk glass surface it seems that an increasing trend exists for cristobalite and devitrite towards the altered compositions of the atmosphere and particularly of the tin bath side and a decreasing trend for β-wollastonite. From extensive analytical investigations with the help of an electron microprobe equipment (see section 2.) it is evident that the glass surface at the tin bath side has a lower Na_2O, CaO and a lower SiO_2 concentration combined with a certain amount of tin oxide (table 2). A similar change of the glass surface at the atmosphere side was found with the following differences: very low tin oxide concentration and somewhat lower concentration of Na_2O and CaO than in the case of the tin bath side and therefore a somewhat larger SiO_2 content (table 2). These alterations in composition are responsible for the differences of the crystal growth rate values between the bulk and the two surfaces of the float glass.

This shift in crystal growth rates with change of composition is not comparable with literature data of glasses from the pure three-component system $Na_2O–CaO–SiO_2$, in which Dietzel [18] in addition did not observe devitrite but only cristobalite and wollastonite, both with 10-fold larger growth rates. The reason for these different results is obviously the different composition (in wt%) of the float glass (table 2) particularly the additional components

Table 2. Relative alterations of the main components (in wt%) at the surfaces of the float glass[2]) as compared with those of the bulk glass and relative changes of crystal growth rate, Δv. Composition of the bulk glass (in wt%): 71.6 SiO_2, 0.6 Al_2O_3, 9.4 CaO, 4.0 MgO, 13.9 Na_2O, 0.16 K_2O, 0.1 Fe_2O_3, 0.05 TiO_2, 0.24 SO_3, 0.03 Cl^-

component	relative alterations in wt%		furnace atmosphere	crystal phase	Δv[3])	
	tin bath side	atmosphere side			tin bath side	atmosphere side
SiO_2	−1.6 to −2.4	+1.6 to +2.0	air	cristobalite	⇓	⇓
CaO	−0.5	−0.75		devitrite	⇓	⇑
Na_2O[4])	−1.6	−1.0 to −2.2	N_2/H_2	cristobalite	n.a.	⇓
Sn_2O_3	+3.3	–		devitrite	⇓	⇑

[2]) The information depth is 1 to 2 μm.
[3]) Arrow down means: smaller crystal growth rate compared with that of the bulk surface, arrow up means: larger values and n.a. means: no alteration. In the case of devitrite Δv means Δv at the maximum growth rate.
[4]) The decrease of this concentration may be somewhat larger. In general, the sodium depletion depends on the manufacturing conditions of the float glass, so the larger decrease of the Na_2O concentration measured by Matoušek and Maryška [5] (−7 %) might be explained in this way. In this connection it is referred to figure 2 and the text with respect to it.

Al_2O_3 and MgO as compared with the pure three-component glass even with the apparently comparable concentrations: 72.3 SiO_2, 13.4 CaO, 14.1 Na_2O; if $Al_2O_3 + Fe_2O_3 + TiO_2$ are added to SiO_2, MgO to CaO and K_2O to Na_2O. These differences in compositions between the real float glass and the mentioned three-component glass give rise to the different results of the alterations of the crystal growth rates, v, when the Na_2O and CaO concentration is decreased and that of SiO_2 is increased on the atmosphere side.

As a conclusion one may state that relatively small changes of glass compositions can lead to drastic changes of the crystallization kinetics, but not – or only to a small degree – of the thermal activation of the crystallization process as was shown from the comparison of the enthalpies at the beginning of section 4.1.

4.2. Influence of redox conditions on crystal growth

Redox conditions have also an influence on the crystallization behaviour at the surfaces of float glass as is seen particularly from the large enthalpy value of cristobalite at the tin bath side under oxidizing conditions and from the fact that β-wollastonite is formed only in a reducing atmosphere (table 1). Obviously, this influence is connected with the superficial immiscibility on the tin bath side under oxidizing conditions and may be related to a redox reaction of the tin ions. Starting from the reducing condition of the float glass process a local oxidation reaction according to equation (1) would be expected as soon as the float glass plate is transferred into the oxidizing atmosphere (air) in a still hot condition.

$$SnO + 1/2\ O_2 \rightleftarrows SnO_2\ . \tag{1}$$

The redox reaction type:

$$Sn^{2+} + 2\ Me^+ \rightleftarrows Sn^{4+} + 2\ Me^0 \tag{2}$$

reported by Shelby and Vitko [19] and Matoušek and Maryška [8] in the case of silver and copper for Me could be expanded by the minor component iron supporting the change of Sn^{2+} to the Sn^{4+} state

$$Sn^{2+} + 2\ Fe^{3+} \rightleftarrows Sn^{4+} + 2\ Fe^{2+} \tag{3}$$

which was recently reported by Kumar, Singh and Pyare [20]. This redox reaction was determined by the authors not with float glass but with a sodium–metasilicate glass. In order to verify equation (3) also for float glass compositions, a series of glasses with float glass compositions were melted in an electrically heated furnace (air atmosphere) with additions (in wt%) of 0.3 FeO and Fe_2O_3 each and with additions of 0.25 SnO + 0.15 FeO; 0.25 SnO_2 + 0.15 Fe_2O_3; 0.25 SnO + 0.15 Fe_2O_3 and 0.25 SnO_2 + 0.15 FeO. In all cases of combinations it was found that an oxidation of $Sn^{2+} \rightarrow Sn^{4+}$ and a reduction of $Fe^{3+} \rightarrow Fe^{2+}$ take place in oxidizing furnace atmosphere (table 3). Examples are given in the spectral diagrams of figure 15. From table 3 it is evident that the introduction of FeO gives only slightly more Fe^{2+} than Fe^{3+} concentration which can be seen from the last column where the ratio of the extinction, E, of Fe^{2+} and of Fe^{3+}, $E(Fe^{2+})/E(Fe^{3+})$, is directly proportional to the ratio of $[Fe^{2+}]/[Fe^{3+}]$ concentration with respect to the Lambert-Beer law:

$$E = \frac{1}{d} \ln \frac{I_0}{I} = \varepsilon \cdot c \tag{4}$$

from which follows:

$$\frac{E(Fe^{2+})}{E(Fe^{3+})} = \frac{\varepsilon(Fe^{2+})}{\varepsilon(Fe^{3+})} \frac{c(Fe^{2+})}{c(Fe^{3+})} = \text{const} \frac{[Fe^{2+}]}{[Fe^{3+}]}\ . \tag{5}$$

From table 3, last column, it is further evident that with the introduction of SnO_2 and preferably of SnO increasingly more Fe^{2+} and decreasingly Fe^{3+} concentration is found. Thus, for the float glass process

Table 3. Results of spectroscopic investigations on the mutual redox interaction of tin and iron in glass melts with float glass composition. Furnace atmosphere: air

glass no.	additions to the batch in wt%				$E(Fe^{2+})$	$E(Fe^{3+})$	$E(Fe^{2+})/E(Fe^{3+})$
	Fe_2O_3	FeO	SnO_2	SnO			
1	0.30	–	–	–	0.851	0.504	1.576
2	–	0.30	–	–	1.072	0.633	1.694
3	–	0.15	0.25	–	0.622	0.219	2.838
4	0.15	–	0.25	–	0.523	0.138	3.790
5	–	0.15	–	0.25	0.890	0.214	4.160
6	0.15	–	–	0.25	0.796	0.187	4.260

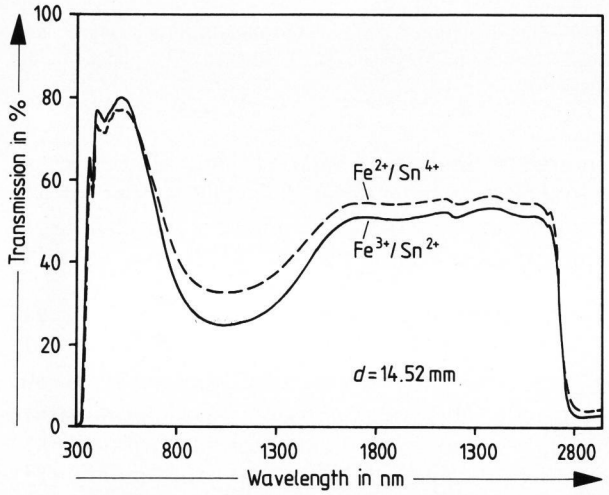

Figure 15. Spectral transmission curves of glasses with float glass composition doped with (in wt%): 0.15 Fe_2O_3 + 0.25 SnO (solid curve) and 0.15 FeO + 0.25 SnO_2 (dashed curve) (see also table 3).

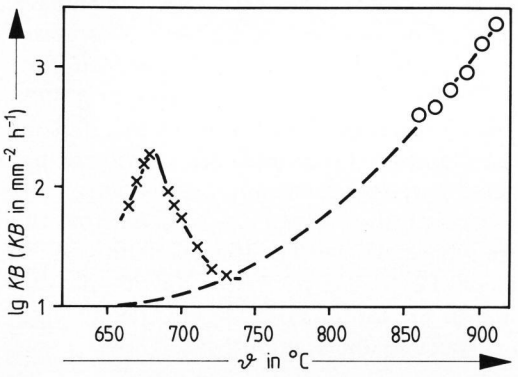

Figure 16. Thermal expansion curves of 5 wt% tin oxide-containing glasses with float glass composition melted in oxidizing (air) and reducing (N_2/H_2 = 99/1) atmosphere.

one can state that reactions take place preferably in the direction

$$Sn^{2+} \rightarrow Sn^{4+} + 2e^- , \quad (6)$$

$$Sn^{2+} + 2\,Fe^{3+} \rightarrow Sn^{4+} + 2\,Fe^{2+} \quad (7)$$

when the float glass leaves the reducing tin bath region. This may be the reason that in the literature there does not exist a clear opinion about the redox condition of tin in float glass [21 to 24] because of the more or less completeness of the reactions (equations (6 and 7)) which depends on the many individual process parameters of the float glass production within a plant and at different plants.

The superficial phase-separated Sn^{4+}-rich sections are expected to have a lower surface tension than the Sn^{2+}-rich ones and spread above the Sn^{2+}-rich boundaries during the immiscibility process. This mechanism contracts the original surface and collects within the special sites of crystallization probably some solid impurity particles. Due to this fact the tin bath side crystallization of cristobalite is hindered. This is reflected by the strong temperature dependence of the growth rates, an altered crystal morphology (figure 8) and the high activation enthalpy indicating a changed growth mechanism. Microanalytical investigations are needed to prove this suggestion, because no definite results were obtained from a fluorescence-microscopic observation.

In connection with the oxidation process (equations (6 and 7)) the wavy shrinking structure of the glass surface at the tin bath side, called "bloom" (figure 13), may be explained as follows. The Sn^{2+} ion in the surface layer of the samples which are annealed in air is oxidized to Sn^{4+}. This leads obviously to a lower thermal expansion and to a higher glass transition temperature, T_g, because the Sn^{4+} ion has a network-forming character. The evidence is given in figure 16 which shows the thermal expansion curves of two glasses with nearly float glass composition (in wt%: 67.9 SiO_2, 0.6 Al_2O_3, 9.1 CaO, 4.0 MgO, 13.4 Na_2O, 5.0 SnO/SnO_2) one of the two glasses melted in an electrically heated furnace in air, the other one in a reducing atmosphere (N_2/H_2 = 99/1). The T_g values are 586 and 576 °C, respectively, the thermal expansion coefficients $\alpha_{(100-400)} = 10.0$, $\alpha_{(350-500)} = 10.7 \cdot 10^{-6}/K$ ("SnO_2 glass") and $\alpha_{(100-400)} = 10.3$, $\alpha_{(350-500)} = 11.3 \cdot 10^{-6}/K$ ("SnO glass"), respectively. Therefore, the bulk glass of the real float glass contracts more than the oxidized leather-like harder and predominantly SnO_2-containing surface layer around and at T_g which leads to

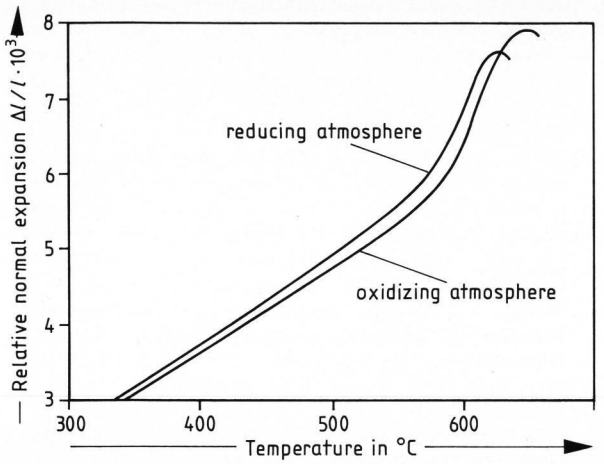

Figure 17. Surface nucleation rate of cristobalite in air at the atmosphere side of float glass versus temperature. ×: after very long induction times, ○: initial rates after unmeasurable short induction times (see figure 12).

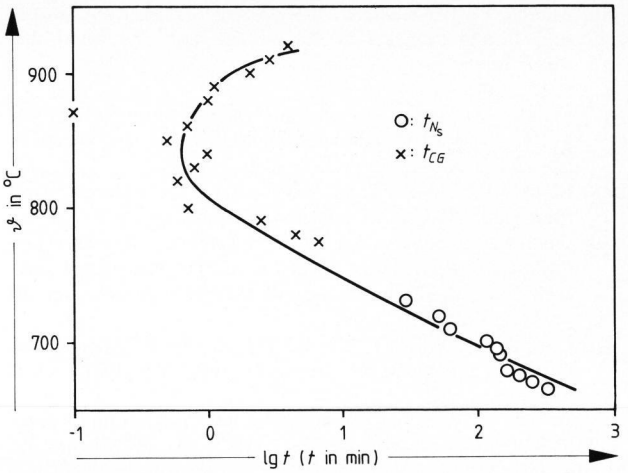

Figure 18. TTT diagram, nucleation and crystallization of cristobalite in air at the atmosphere side of float glass. ×: induction times t_{CG}, from crystal growth rates, ○: induction times, t_{N_s}, from heterogeneous nucleation rates.

the observed wavy shrinking surface structure. But also the deeper layers which may be still SnO-rich contribute to this effect because even the "SnO glass" has a higher T_g value (576 °C) than the bulk float glass (550 °C). In addition to these effects the oxidation itself (equations (1 and 6)) produces a certain increase of the surface volume by the incorporation of oxygen and may support the "bloom" phenomenon slightly.

4.3. Nucleation

The nucleation rates of cristobalite at the atmosphere side of the float glass corresponding to N_s, given by the slope of the graphs in figure 12, indicate a division into two parts (figure 17). At elevated temperatures, the surface nucleation rates are very high and crystallization arises from a fixed number of special sites which obviously depends on the surface conditions. The enhanced nucleation rates determined from the slope of a tangential construction in figure 12 are the result of a catalytic effect of impurity particles on the surface as recently suggested by Zanotto [25].

At lower temperatures, however, the latter mechanism is no longer dominant and the nucleation rates show a maximum of considerably smaller amount. The time and temperature dependence of N_s contradicts the measurements of Zanotto [25]: He did not distinguish between the tin bath and the atmosphere side and determined an activation enthalpy for devitrite (N_s up to 3000 mm^{-2}) to be 135 kJ/mol although this value had not been reported in previous research as was discussed in section 4.1. (compare also table 1). Additionally, he measured no induction periods for crystallizations at temperatures between 750 and 800 °C and induction times with very large scatter (up to 50 h) in the case of N_s versus t plots. Such large values have not been observed in the present work.

In figure 18 a TTT (Time-Temperature-Transformation) diagram is shown, connecting the growth induction times of cristobalite at the atmosphere side with the induction times of the corresponding heterogeneous nucleation. With respect to the first data, the small post-growing time of at least 2 min had been subtracted. Devitrification starts with the crystallization of cristobalite and this is reflected within the limits of the graph.

In this paper no further nucleation experiments on the tin bath and bulk glass surface were carried out. The time and temperature dependence of the number of devitrite and β-wollastonite crystals had not been studied because of the low values of N_s.

*

The authors are grateful for samples from and discussions with Dr. Rädisch and Dr. Küstner, VEGLA, Herzogenrath (FRG), to Dr. Merker, Flachglas AG, Gelsenkirchen (FRG), and to Dr. Helfmeier and Dr. Galbert, ZELMI, TU Berlin (FRG), for the electron microprobe analyses as well as to Mrs. Sauer and Mrs. Gärtner, Institut für Nichtmetallische Werkstoffe, TU Berlin, for the spectroscopic and thermal expansion measurements and preparation of the SnO_x-containing glasses.

5. References

[1] Brückner, R.; Fernández Navarro, J.: Spannungen und Ionentransport im Floatglas. Glastech. Ber. **44** (1971) no. 9, p. 361–368.
[2] Sieger, J. S.: Chemical characteristics of float glass surfaces. J. Non-Cryst. Solids **19** (1975) p. 213–220.
[3] Zhi Hong-Liang; Cooper, A. R.: Effect of atmosphere and temperature on the equilibrium between molten tin and soda-lime glass. J. Am. Ceram. Soc. **68** (1985) no. 8, p. C195–C196.
[4] Hessenkemper, H.; Brückner, R.: Unpubl. work.
[5] Matoušek, J.; Maryška, M.: Chemical composition of the float glass surface. Sklář Keram. **40** (1990) p. 337–340.

[6] Manns, P.; Brückner, R.: Biegefestigkeit von Kalk-Natron- und Borosilicatglas von Raumtemperatur bis zur Littleton-Temperatur. Glastech. Ber. **56** (1983) no. 6, p. 155–164.
[7] Merker, L.: Einfacher Nachweis örtlicher Abweichungen des Fe^{2+}/Fe^{total}-Verhältnisses in technischen Gläsern. Glastech. Ber. **54** (1981) no. 6, p. 201–204.
[8] Matoušek, J.; Maryška, M.: Diffusion in the surface layer of float glass. Silikaty **35** (1991) p. 43–51.
[9] Gebhardt, F.; Graff, U.; Merker, L. et al.: Wasserbeständigkeit von Kalk-Natronsilicatgläsern. Vergleichende Untersuchungen an Glasgrieß und Glasplatten. Glastech. Ber. **54** (1981) no. 8, p. 257–264.
[10] Gebhardt, F.; Graff, U.: Beitrag zur Verflüchtigung von Alkalien aus Floatglas. Glastechn. Ber. **54** (1981) no. 1, p. 1–7.
[11] Flörke, O. W.: Strukturanomalien bei Tridymit und Cristobalit. Ber. Dtsch. Keram. Ges. **32** (1955) no. 12, p. 369–381.
[12] Pilkington, L. A. B.: The float glass process. Proc. R. Soc. London **A 314** (1969) p. 1–25.
[13] Dietzel, A., Wickert, H.: Der Verlauf der Glasigkeit im System Na_2O-SiO_2. Glastech. Ber. **29** (1956) no. 1, p. 1–4.
[14] Schönborn, H.: Die Eigenschaften von porösem Sinterglas. Silikattechnik **13** (1962) no. 12, p. 419–424.
[15] Dietzel, A.; Flörke, O. W.: Gleichgewichtszustände in flüssigem Glas. Glastech. Ber. **28** (1955) no. 11, p. 423–426.
[16] Swift, H. R.: Some experiments on crystal growth and solution in glasses. J. Am. Ceram. Soc. **30** (1947) no. 6, p. 165–169.
[17] Kuan-Han Sun: Fundamental condition of glass formation. J. Am. Ceram. Soc. **30** (1947) no. 9, p. 277–281.
[18] Dietzel, A.: Die Kristallisationsgeschwindigkeit der technischen Natron-Kalk-Silikatgläser. Sprechsaal **62** (1929) p. 506–509; 524–525; 543–544; 562–568; 584–585; 603–604; 619–621; 638–639; 657–660.
[19] Shelby, J. E.; Vitko, J. jr.: Colloidal silver formation at the surface of float glass. J. Non-Cryst. Solids **50** (1982) p. 107–117.
[20] Kumar, A.; Singh, S. P.; Pyare, R.: $Sn^{2+}-Sn^{4+}$ and $Fe^{2+}-Fe^{3+}$ redox interaction in 30 $Na_2O-70\,SiO_2$ glass. Glastech. Ber. **64** (1991) no. 4, p. 106–108.
[21] Merker, L.: Spezielle chemische Wechselwirkungen beim Floatglas. In: Jebsen-Marwedel, H.; Brückner, R. (eds.): Glastechnische Fabrikationsfehler. 3rd. ed. Berlin, Heidelberg, New York: Springer 1980. p. 496–498.
[22] Suscavage, M. J.; Pantano, C. G.: Tin penetration into a soda–lime–magnesia–silica glass. Glastech. Ber. **56K** (1983) Bd. 1, p. 498–503.
[23] Stegemann, G.; Lengeler, B.; Stanglmeier, F. et al.: X-ray absorption spectroscopy in total reflection. A novel tool for the characterization of glass surfaces. In: Mazurin, O. V. (ed.): XV International Congress on Glass, Leningrad 1989. Vol. 2a. Leningrad: "Nauka" Leningrad Branch 1989. p. 119–123.
[24] Jie Luo; Chao Xu: XPS examination of tin oxide on float glass surface. J. Non-Cryst. Solids **119** (1990) no. 1, p. 37–40.
[25] Zanotto, E. D.: Surface crystallization kinetics in soda–lime–silica glasses. J. Non-Cryst. Solids **129** (1991) no. 1–3, p. 183–190.

92R0738